https://doi.org/10.15407/ufm.23.02.239

O.V. KHOMENKO*, A.A. BIESIEDINA, K.P. KHOMENKO, and R.R. CHERNUSHCHENKO
Sumy State University,
2 Rimsky-Korsakov Str., UA-40007 Sumy, Ukraine
* o.khomenko@mss.sumdu.edu.ua

COMPUTER MODELLING OF METAL NANOPARTICLES ADSORBED ON GRAPHENE

The influence of deposited Al, Pd, Co, Au, Ni atoms on a single-layer graphene substrate is investigated using computer simulations. The computer modelling of spraying nanoparticles on the basis of molecular dynamics method is implemented using the NVIDIA®CUDA™ technique. According to the results of model calculations, the general behaviour of the system is investigated. The experiments are performed to study the sputtering of atoms of different metals under different initial conditions of the system. Based on these sprays, the behaviour at the beginning of the interaction of the deposited atoms with the substrate is analysed. The time dependences of the lateral position of nanoparticles' centre of mass and the substrate force throughout the experiment for different sprayed materials are compared. The behaviour of total and potential energies, temperature and momentum of the system is studied. As shown, there is a jump in total energy and temperature as well as a change in the behaviour of the momentum and the substrate force when carbon atoms of graphene are reached for all depositions.

Keywords: computer model, molecular dynamics, sputtering, graphene, nanoparticle, atomic force microscopy.

1. Introduction

Modern science and technology set goals for the development and creation of new high-performance materials and technologies (nanomaterials, nanotechnologies) and technological equipment based on the fundamental physical laws of interaction of micro- and nanoparticles, which determine the structure and properties of structural materials in operation conditions [1–30]. Physics, studying the processes and phenomena

Citation: O.V. Khomenko, A.A. Biesiedina, K.P. Khomenko, and R.R. Chernushchenko, Computer Modelling of Metal Nanoparticles Adsorbed on Graphene, *Progress in Physics of Metals*, **23**, No. 2: 239–267 (2022)

that occur in various real systems of a large number of bodies and in individual bodies, considers the structure and properties of solids as some variable characteristics.

Since the discovery of graphene, two-dimensional materials have increasingly attracted the attention of scientists around the world. Increased interest in these materials is due to their unique structure, because these samples have a thickness of several atomic layers, which also determines their unique properties, and therefore opens a wide potential for their application in many fields of science and technology. The study of the parameters of two-dimensional nanomaterials by experimental methods is a much more difficult task, which is why it is advisable to use computer modelling.

In addition, there is a growing interest in the literature on the interaction of graphene sheets with various nanoobjects, which confirms the relevance of the work. The obtained results and developments can be used in further theoretical and experimental studies. It is also known that nanoparticles can affect the electronic and structural properties of carbon, which may contribute to the invention and improvement of nanodevices in the future.

The present review work deals with studying and analysing the behaviour and influence of sputtering metal atoms on a single-layer graphene substrate using computer simulation. Computer model of the sputtering nanoparticles by the molecular dynamics method is implemented through the NVIDIA®CUDA™ technique.

2. Manipulation and Computer Simulation of Metal Nanoparticles Adsorbed on Surfaces

2.1. Atomic-Force Microscopy, Principle of Action and Research Methods

The invention of friction and atomic force microscopy (AFM) allowed us to study tribological phenomena in dry nanocontacts. With the use of AFM and friction force microscopy techniques, it is possible to experiment on them. Experimental study of microcontacts of surfaces separated by a thin film of liquid is carried out using a surface force apparatus. Often, as materials for work surfaces, graphite is used in AFM and friction force microscopy, and in surface force apparatus, it is mica. These materials have a layered structure, which makes it possible to obtain atomically smooth surfaces [1, 7].

AFM was invented in 1986. Its work is based on the force interaction of the probe and the surface. To register this interaction, special probe sensors are used (Fig. 1). The force acting on the probe from the side of the surface causes the console to bend. When registering the

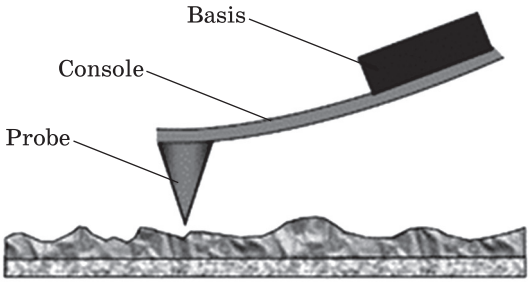

Fig. 1. The scheme of the probe sensor

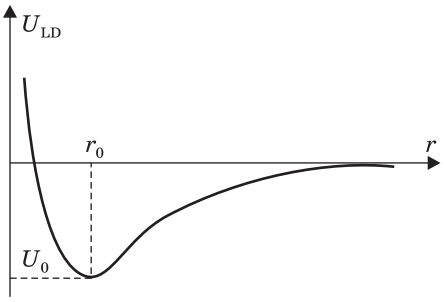

Fig. 2. Qualitative view of Lennard-Jones potential

amount of bending, it is possible to control the strength of the interaction between the probe and the surface [2].

Consider the forces under which the microscope works. The forces of interaction between the probe and the sample are the short-acting Van der Waals forces. They include components of different signs providing attraction for long distances and repulsion for short ones. Most often, the energy of the Van der Waals interaction, which appears between two atoms at a distance r, is approximated by the power function of the Lennard-Jones potential (Fig. 2):

$$U_{LD} = U_0 \left[-2\left(\frac{r_0}{r}\right)^6 + \left(\frac{r_0}{r}\right)^{12} \right]. \quad (1)$$

In formula (1), the first term characterizes the long-range attraction, and the second term characterizes the repulsion of atoms at short distances. The parameter r_0 is the equilibrium distance between the atoms; U_0 is the energy value in the minimum.

The Lennard-Jones potential makes it possible to assess the strength of the interaction between the probe and the sample. The total energy of the system can be obtained by summing the elementary interactions for each atom of the probe and the sample. Thus, for the energy of interaction we obtain [26]:

$$W = \int_{Vp} \int_{Vs} U_{LD}(r - r') n_p(r) n_s(r') dV dV' . \quad (2)$$

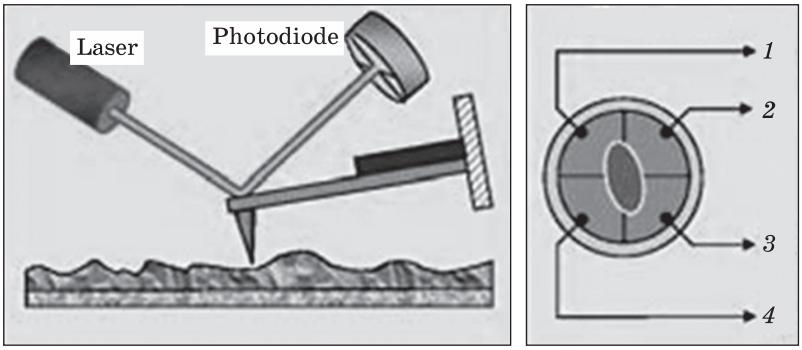

Fig. 3. Scheme of optical bending registration of AFM probe sensor console

In formula (2), $n_p(r)$ and $n_s(r')$ are the densities of the atoms contained in the sample and probe materials. In addition, the force acting on the probe from the surface can be calculated as follows:

$$\mathbf{F}_{ps} = -\text{grad}\, W. \tag{3}$$

The interaction of the probe with the sample in the AFM is more complex, but in any case, it is unchanged that the AFM probe is attracted to the sample at greater distances and repelled at smaller ones. Registration of small bends of the elastic console of the probe sensor is carried out on the basis of optical methods (Fig. 3). The AFM optical system is configured so that the radiation of the semiconductor laser is focused on the probe sensor console, and the reflected beam hits the centre of the photosensitive region of the photodetector. Four-section semiconductor photodiodes are used as position-sensitive photodetectors.

It is also worth noting that the material of the substrate and the film sprayed on it will have a significant impact. Therefore, in different experiments and studies, it is advisable to use different substrates, depending on their chemical structure. The substrate material and its structural state also significantly affect the friction anisotropy [3], magnetoresistive [4], magneto-optical properties and diffusion processes in film systems. For instance, in oriented cultivation on a single crystal MgO(100), the Au(2)/Co(30)/Fe(30)/MgO system shows significant anisotropy of magnetoresistance and coercive force (2 times increasing when rotating the sample by 45°) [5].

Studies of electrodes in which the surface is modified by diamond-like films by AFM methods have shown that the substrate material has a significant effect on the structure of the deposited film. Thus, platinum electrodes that are modified by diamond-like films can be used in a microelectrode analytical system where the coating defects will be insignificant. The use of glass-carbon electrodes coated with nitrogen-

doped diamond-like films, after deposition from vacuum-arc plasma, gave better results. These electrodes will be useful during electrochemical studies. Such electrode systems are characterized by the following advantages: biocompatibility, wide window of working potentials, especially in aqueous solutions, low background currents, the possibility of further surface cleaning, as well as long service life [6].

Consider the existing methods of studying the sample using AFM. The non-contact method of sample surface examination has unique capabilities compared to other probe microscopy methods, such as contact force scanning microscopy and scanning tunnelling microscopy [7]. The absence of repulsive forces in non-contact scanning force microscopy makes it possible to use it in the study of 'soft samples', while in non-contact microscopy, unlike scanning tunnelling microscopy, there is no need for conducting samples.

Non-contact microcircuits use the principle of determining 'amplitude modulation'. The corresponding measurement scheme uses amplitude changes. Fluctuations of the cantilever A is due to the interaction of the probe with the sample. The gradient-force model can be described by the method of contactless microscopy. According to this model, within small A when the cantilever approaches the sample, the resonant frequency of the cantilever f_0 shifts by the value of df to a new value by the expression [10]:

$$f_{eff} = \frac{f_0}{2}\left(1 - \frac{F'(z)}{k_0}\right). \quad (4)$$

In formula (4), f_{eff} is the new value of the resonant frequency of the cantilever with the nominal value of stiffness k_0, and $F'(z)$ is the gradient of the force of interaction of the cantilever with the sample. The value of z is the effective gap of the probe-sample, in the case of gravity $df = f_{eff} - f_0$ is negative.

If the excitation frequency of the cantilever $f_{eff} > f_0$, then a decrease in the resonant frequency causes a decrease in the amplitude of oscillations A_{set} of the cantilever with a frequency f_{set} when approaching the sample. Such changes in amplitude A are used as an input signal to the feedback system. To obtain a scanning image, the contactless method must first select some amplitude A_{set}, with $A_{set} < A(f_{set})$ when the cantilever is at a considerable distance from the surface of the sample. The feedback system moves the cantilever closer to the surface until its instantaneous amplitude A is equal to the amplitude A_{set} at the specified excitation frequency f_{set}. The feedback system moves the cantilever closer to the surface until its instantaneous amplitude A is equal to the amplitude at the specified oscillation excitation frequency. Starting from this point, the scanning of the sample in the xy plane can be started by holding the feedback $A = A_{set} = \text{const}$ to obtain the image. The

feedback system moves the cantilever to the sample, when the A_{set} decreases at any point, and pushes the cantilever away from the sample if the A_{set} increases. In general, as a consequence of the above model within the small A scanned image can be considered as a relief of a constant gradient of the force of interaction of the probe-sample.

The method of non-contact microscopy has the advantage that the probe does not come into contact with the sample, and therefore does not destroy it and does not distort the image. This can be important when studying biological samples. When using non-contact and intermittent contact methods, the cantilever is oscillated at a constant resonant excitation frequency, the force gradients are defined as changes in the amplitude or phase of the oscillation of the cantilever [8]. According to this scheme, the signal-to-noise ratio for a given bandwidth can be increased by increasing the quality factor Q of the oscillations of the cantilever. However, increasing Q simultaneously reduces the maximum possible bandwidth of the system. This fact becomes especially important when working in a vacuum. In vacuum, the quality factor of the cantilever Q can be more than 50 000. Such high Q values provide high sensitivity but low bandwidth (less than 1 Hz), resulting in very low contact force scanning microscopy scan speeds for most applications.

To increase the sensitivity of the contact force scanning microscopy with increasing Q without restrictions on bandwidth or dynamic range, an alternative detection method is proposed, so-called frequency modulation method. In a frequency-modulation detection system, high-quality resonant oscillations of the cantilever are a frequency-defined component of the oscillator that oscillates with constant amplitude. Changes in force gradients cause instantaneous changes in the oscillation frequency of the oscillator, which are determined by the frequency-modulating demodulator. The cantilever is supported by the use of positive feedback, which fluctuates at its resonant frequency, by means of a control amplifier.

Method of studying the surface of a sample of static magnetic force microscopy is an effective tool for the study of magnetic structures at the submicron level. The image obtained by magnetic force microscopy is a spatial distribution of a certain parameter that characterizes the magnetic interaction of the probe and the sample. The magnetic cantilever is a standard silicon probe sensor covered with a film of magnetic material [9]. Magnetic force microscopy makes it possible to study magnetic domain structures with high spatial resolution of recording and reading information in a magnetic environment, remagnetization processes.

2.2. Relevance of the Study of Graphene

Since the discovery of graphene, a huge amount of fundamental, experimental and theoretical research has been performed. This material has an extremely wide range of uses. Due to its high electrical and ther-

mal conductivity, graphene can be used in various electronic devices, especially given its flexibility and complete optical transparency. Carbon is a promising material for the implementation of chips, measuring devices, biosensors, ultracapacitors, flexible displays based on it [10]. Graphene can also be an effective gas sensor that senses the presence of even a single gas molecule on its surface [11].

Unique electronic and transport properties [12–14] make graphene one of the most promising materials in the field of nanoelectronics and spintronics devices and even in electrochemistry [15, 16]. Currently, graphene is being developed in the following areas: high-frequency transistors, memory chips, electrodes for supercapacitors, inexpensive displays for portable devices, batteries for hydrogen fuel vehicles, sensors for disease diagnosis, cooling of electronic circuits.

Two-dimensional materials are increasingly attracting the attention of scientists around the world (see, *e.g.*, Refs. [17–22] and references therein). Increased interest in these materials is due to their unique structure, because these samples have a thickness of several atomic layers, which also determines their unique properties, and therefore opens a wide potential for their application in many fields of science and technology [12–22].

The study of the parameters of two-dimensional nanomaterials by experimental methods is a much more difficult task compared to samples of normal size. This situation is due to the atomically thin structure of two-dimensional nanomaterials; in addition, their surface usually contains functional groups, which further complicates the study of mechanical properties. Numerical modelling and construction of phenomenological models with the subsequent study of dynamic dependencies allow simplifying the task of calculating mechanical parameters considerably. Besides, there is a growing interest on the interaction of graphene with various nanoobjects, as they can change the electronic and structural properties of this material, which may affect the future invention and improvement of nanodevices [23, 24].

2.3. The Principle of Operation of the Program Surface Growth

This subsection presents the features of the model that underlie the work of SurfaceGrowth [25]. In classical molecular dynamics, the potential interaction energy V of atoms plays a key role in modelling a material. For metals, SurfaceGrowth uses an empirical multiparticle potential based on the embedded atom method (EAM) and implemented in works [26, 27]. It is designed for modelling alloys and is fully expressed through analytical functions in contrast to the first versions of EAM, where for the embedding function cubic splines are used [27]. In EAM,

the potential energy V of the crystal can be expressed as follows [26]:

$$V_{eam} = \frac{1}{2}\sum_{i,j,i\neq j}\phi_{ij}(r_{ij}) + \sum_{i}F_i(\rho_i), \tag{5}$$

where ϕ_{ij} represents the pair energy between the atoms i and j, separated by the distance r_{ij}, and F_i means the embedding energy required to place the atom i in the local position with electron density ρ_i, calculated as follows:

$$\rho_i = \frac{1}{2}\sum_{i,j,i\neq j} f_j(r_{ij}), \tag{6}$$

where $f_j(r_{ij})$ is the electron density at the location of i atom, which originates from j atom at the distance r_{ij}. The generalized pair potential has the form:

$$\phi(r) = \frac{A\exp\left[-\alpha\left(\frac{r}{r_e}-1\right)\right]}{1+\left(\frac{r}{r_e}-k\right)^{20}} - \frac{B\exp\left[-\beta\left(\frac{r}{r_e}-1\right)\right]}{1+\left(\frac{r}{r_e}-\lambda\right)^{20}}, \tag{7}$$

where r_e is the equilibrium distance between the nearest neighbours, A, B, α, β are the fitting parameters, and k, λ are two additional parameters for the cut-off. The electron density function has the same shape as the term of attraction in the pair potential with the same values of β and λ, that is:

$$f(r) = \frac{f_e\exp\left[-\beta\left(\frac{r}{r_e}-1\right)\right]}{1+\left(\frac{r}{r_e}-\lambda\right)^{20}}. \tag{8}$$

For the embedding function F to work for a wide range of electron density values, three equations are used for each of the following intervals: $\rho < \rho_n$, $\rho_n \le \rho < \rho_0$ and $\rho_0 \le \rho$. Taking into consideration that $\rho_n = 0.85\rho_e$, where ρ_e is the equilibrium electron density, you can be sure that all equilibrium properties can be obtained in the range of electron density $\rho_n \le \rho < \rho_0$. For smooth change of embedding energy, the equations giving identical values of function and its derivative on limits of intervals are required. These equations have the form:

$$F(\rho) = \sum_{i=0}^{3} F_{ni}\left(\frac{\rho}{\rho_e}-1\right)^i,\ \rho < \rho_n,\ \rho_n = 0.85\rho_e, \tag{9}$$

$$F(\rho) = \sum_{i=0}^{3} F_i\left(\frac{\rho}{\rho_e}-1\right)^i,\ \rho_n \le \rho < \rho_0,\ \rho_0 = 1.15\rho_e, \tag{10}$$

$$F(\rho) = F_e\left[1 - \ln\left(\frac{\rho}{\rho_e}\right)\right]\left(\frac{\rho}{\rho_e}\right)^{\eta},\ \rho_0 \le \rho. \tag{11}$$

The values of the parameters included in all written equations for 16 metals can be found in Ref. [27], or for six metals in the SurfaceGrowth code. The values of density and mass of metals in SurfaceGrowth are taken from the book [28], where you can also find other characteristics of metals.

The force acting on the k atom by other metal atoms is given by the expression:

$$f_k = -\frac{\partial V_{eam}}{\partial \mathbf{r}_k} = -\sum_{j\neq k}\frac{d\,\phi(r_{kj})}{dr}\hat{\mathbf{r}}_{kj} - \sum_{i=1}^{N_m}\frac{\partial F_i}{\partial \rho_i}\frac{\partial \rho_i}{\partial \mathbf{r}_k}, \tag{12}$$

where N_m is the total number of metal atoms, $\hat{\mathbf{r}}_{kj}$ is a unit vector directed from atom j to atom k. Expressions for derivatives in Eq. (12) have the form:

$$\frac{d\phi}{dr} = \frac{A\exp\left[-\alpha\left(\frac{r}{r_e}-1\right)\right]}{1+\left(\frac{r}{r_e}-\kappa\right)^{20}}\left[\alpha + \frac{20\left(\frac{r}{r_e}-\kappa\right)^{19}}{1+\left(\frac{r}{r_e}-\kappa\right)^{20}}\right]\frac{1}{r_e} +$$

$$+\frac{B\exp\left[-\beta\left(\frac{r}{r_e}-1\right)\right]}{1+\left(\frac{r}{r_e}-\lambda\right)^{20}}\left[\beta + \frac{20\left(\frac{r}{r_e}-\lambda\right)^{19}}{1+\left(\frac{r}{r_e}-\lambda\right)^{20}}\right]\frac{1}{r_e}; \tag{13}$$

$$\sum_{i=1}^{N_m}\frac{\partial F_i}{\partial \rho_i}\frac{\partial \rho_i}{\partial \mathbf{r}_k} = \sum_{i=1,i\neq k}^{N_m}\frac{df(r_{ki})}{dr}\left(\frac{\partial F_i}{\partial \rho_i} + \frac{\partial F_k}{\partial \rho_k}\right)\hat{\mathbf{r}}_{ki}; \tag{14}$$

$$\frac{df}{dr} = -\frac{f_e\exp\left[-\beta\left(\frac{r}{r_e}-1\right)\right]}{1+\left(\frac{r}{r_e}-\lambda\right)^{20}}\left[\beta + \frac{20\left(\frac{r}{r_e}-\lambda\right)^{19}}{1+\left(\frac{r}{r_e}-\lambda\right)^{20}}\right]\frac{1}{r_e}; \tag{15}$$

$$\frac{dF}{d\rho} = \frac{1}{\rho_n}\left[F_{n1} + 2F_{n2}\left(\frac{\rho}{\rho_n}-1\right) + 3F_{n3}\left(\frac{\rho}{\rho_n}-1\right)^2\right],\ \rho < \rho_n,\ \rho_n = 0.85\rho_e; \tag{16}$$

$$\frac{dF}{d\rho} = \frac{1}{\rho_e}\left[F_1 + 2F_2\left(\frac{\rho}{\rho_e}-1\right) + 3F_3\left(\frac{\rho}{\rho_e}-1\right)^2\right],\ \rho_n \le \rho < \rho_0,\ \rho_0 = 1.15\rho_e; \tag{17}$$

$$\frac{dF}{d\rho} = -\frac{F_e \eta}{\rho_e}\left(\frac{\rho}{\rho_e}\right)^{\eta-1} \ln\left(\frac{\rho}{\rho_e}\right)^{\eta}, \ \rho_0 \le \rho. \tag{18}$$

Since the expression for the potential energy of a metal (5) and the force acting on a metal atom (12) consists of two parts: a paired part, depending on the relative position of the atoms, and the EAM part, which depends on the electron density of all atoms other than this, then the calculation of V_{eam} and force is done in two stages. First, the electron density is calculated for each atom, and then these values.

The potential energy V_C of interacting C atoms in the graphene layer is described by the following spring potential from Ref. [29]:

$$V_C = \frac{1}{2}\left\{\sum_{i-j}\mu_r(r_{ij}-r_0)^2 + \sum_{i-j-k}\mu_0 r_0^2(\theta_{ijk}-\theta_0)^2 + \sum_{i-(j,k,l)}\mu_p\left(\delta z_i - \frac{\delta z_j + \delta z_k + \delta z_l}{3}\right)^2\right\}. \tag{19}$$

The sum is made for the nearest neighbours, their pairs and triplets, and the values of the parameters can be found in Ref. [29]. Make an expression for the force acting on a carbon atom and on the part of other atoms in the carbon layer:

$$\mathbf{f}_i = -\sum_{i-j}\mu_r(r_{ij}-r_0)\frac{\mathbf{r}_{ij}}{r_{ij}} + \sum_{j\ne i,k\ne i}\mu_\theta r_0^2(\theta_{jik}-\theta_0)\left[1-\left(\frac{\mathbf{r}_{ij}\mathbf{r}_{ki}}{r_{ji}r_{ki}}\right)^2\right]^{-\frac{1}{2}} \times$$

$$\times \frac{\left(1-\frac{r_{ji}}{r_{ki}}\cos\theta_{jik}\right)\mathbf{r}_{ik} + \left(1-\frac{r_{ki}}{r_{ji}}\cos\theta_{jik}\right)\mathbf{r}_{ij}}{r_{ji}r_{ki}} +$$

$$+ \sum_{j\ne i,k\ne i}\mu_\theta r_0^2(\theta_{ijk}-\theta_0)\left[1-\left(\frac{\mathbf{r}_{ij}\mathbf{r}_{kj}}{r_{ij}r_{kj}}\right)^2\right]^{-\frac{1}{2}}\left[\frac{\mathbf{r}_{kj}}{r_{ij}r_{kj}} - \frac{(\mathbf{r}_{ij}\mathbf{r}_{kj})}{r_{ij}^3 r_{kj}}r_{ij}\right] -$$

$$- \sum_{j,k,l}\frac{2}{3}\mu_\rho\left[2\delta z_i - (\delta z_j + \delta z_k + \delta z_l)\right] - \frac{1}{9}\mu_\rho\sum_{m,n}(\delta z_m + \delta z_n). \tag{20}$$

In the latter sum, the indices m and n denote the neighbours of atom i, following the nearest. Thus, when calculating the force from the spring potential, it is necessary to consider not only the three nearest neighbours in the graphene layer, but also the neighbours of the nearest neighbours, which is taken into account in the program code.

The metal–carbon interaction is described by the Lennard-Jones potential:

$$V_{LJ} = \begin{cases} 4\varepsilon\left[\left(\frac{\sigma}{r}\right)^{12} - \left(\frac{\sigma}{r}\right)^{6}\right], & r < r_c, \\ 0, & r \ge r_c, \end{cases} \tag{21}$$

where the default values of the parameters ε and σ are selected as in Ref. [29], but the program interface allows you to set these values. The cut-off distance is equal to $r_c = 2.5\sigma$. Do a notice that the cut-off distance $r_c = 1.45a$ is used for the EAM potential, and a is the lattice constant of the metal.

3. Results and Discussion

3.1. Description of the Program for Analysis of the Obtained Sputtering

In the program SurfaceGrowth, modelling is performed in three modes: 'Bulk', 'Surface Growth', 'Shear'. They differ in the content of atoms, their initial position, the course of calculations and the possibility of change [25].

In the 'Surface Growth' mode, you can investigate the sputtering of the atoms of the selected metal on the graphene layer by adjusting the sputtering energy of the metal atoms, temperature, flux density of the sputtered atoms, and the parameters of the metal–carbon interaction. The algorithm of calculations in the 'Surface Growth' mode is as follows. The size of the graphene sheet and the number of metal atoms are specified. Initially, in the modelling area there is only a graphene layer placed parallel to the xy plane, and the metal atoms are in the modelling area and do not interact with each other. Periodic boundaries are applied in the xy plane. The boundary atoms around the perimeter in the graphene substrate are rigidly fixed so that the layer does not shift in the vertical direction parallel to the z axis. After an equilibration period, the user sets the duration of which and during which the set value of the graphene layer temperature is reached, through the number of time steps specified by the user, metal atoms are introduced into the modelling area above the graphene layer by groups whose size is also set.

The introduced atoms have random coordinates in the xy plane; their z coordinate is determined by the size of the simulation area. The components x and y of the initial speeds of the embedded metal atoms are equal to 0, and the z component is directed to the graphene layer (against the z axis) and its value is determined by the expression:

$$v_{0z} = \sqrt{\frac{2\varepsilon_{dep}}{m}}, \tag{22}$$

where ε_{dep} is the energy of the sputtered atom specified by the user, m is the mass of the metal atom.

In the 'Surface Growth' mode, you can measure general parameters. Note that the Berendsen thermostat, which is used to remove heat [30], is applied only to carbon atoms and too intense bombardment of the graphene layer will lead to its overheating and destruction. Therefore,

this mode requires a very careful selection of parameter values, as high values of atomic energy or flux density lead to the destruction of the graphene layer.

In the application, you can make measurements of various system parameters: general parameters and characteristics of the nanoparticle. If the user has made the appropriate choice, the general parameters are displayed in a text file through the number of time steps specified by the user. This number also determines the interval over which quantities are averaged. General parameters include:

• stepCnt — the number of time steps that have passed since the beginning of the simulation;

• impulse — full impulse of the system;

• totEn (eV), totEn.rms (eV) — the total energy of the system and its standard deviation (in electron volts) for the averaging period; the total energy is equal to the sum of the potential and kinetic energies of all atoms;

• potEn (eV), potEn.rms (eV) — potential energy of the system and its standard deviation (in electron volts), the first equals the sum of the potential energies of all atoms;

• Tempr (K), T.rms (K) — system temperature and its standard deviation (in Kelvin degrees) for the averaging period, calculated based on the kinetic energy of atoms; in the 'Shear mode', when calculating the sum of the squares of the velocities, the velocity of the centre of mass is subtracted from the velocity of each metal atom to eliminate this contribution to temperature;

• oneStep (ms) — the average duration of the calculation of the time step in milliseconds.

• Most of the characteristics of the nanoparticle are output to the same text file as the general parameters. The characteristics include:

• Veloc_CM — the velocity of the centre of mass (CM) of the nanoparticle along the x-axis;

• X_{CM} (angstr) — the CM coordinate of the nanoparticle along the x direction (in angstroms); the origin is in the centre of the simulation area;

• friction (nN) — the substrate force acting on the particle (in nanonewtons); it is equal to the x component of the force acting on the metal atoms by the carbon atoms [31].

The model considers a substrate consisting of a two-dimensional graphene layer that is subjected to low-energy atomic particle bombardment. We investigated such sputtering materials as Al, Pd, Pt, Au, Co and Ni atoms. The sputtering procedure was simulated using the SurfaceGrowth program with basic settings as follows:

(i) operating mode is the 'Surface Growth';

(ii) selected sputtering material (all listed earlier);

(iii) the size of the substrate is 64×64 cells;
(iv) temperature is of 100 K;
(v) the number of sputtered atoms is of 10 000;
(vi) the number of sputtering steps is of 1 500 000;
(vii) atomic deposition energy is of 0.03 eV;
(viii) time step is of 0.5 ms.

The sputtered atoms directed to the surface could interact with each other before approaching the surface.

Approximately, in half of the simulated sputtering in 1 500 000 steps uneven placement of atoms can be observed. Finally, we observe atomistic images in which atoms are grouped. Such formations are visible both above the substrate and after passing through it. When atoms approach the graphene layer, most of them pass through it without hindrance, the rest linger on the surface. In addition, when the graphene layer is bombarded with atoms, deformation can be observed, but the destruction of the substrate is not observed. As the temperature increases, the substrate will collapse at lower values of the energy of the bombarding particles [31, 32]. That is, increasing the temperature reduces the resistance of the carbon sheet to damage.

3.2. System Model Behaviour

Understanding the friction and wear of graphene that interacts with different materials is useful because these processes are often associated with production. One such application of carbon is sensors that can detect the type and concentration of toxic gases that are needed in various environments and industries [33]. Pure graphene is a good conductor, but inactive for gas trapping, because there are only a few functional groups on its surface, which limits the chemisorption of the gas molecule [34]. Reduced graphene oxide has a rapid and high response to gas molecules at room temperature [35]. However, the disadvantage of such reduced graphene oxide gas sensors is the long recovery time due to the high bond strength between gas molecules and graphene material [36]. Metal oxide semiconductors, which are decorated with precious metals such as Pd or Pt, improve the sensitivity, recovery time and operating temperature of metal oxide/reduced graphene oxide systems [37, 38].

Therefore, to study the properties and new areas of use of graphene, we analyse the effect of low-energy bombardment by atoms of various materials on the substrate surface. Consider the changes in the system for each of the sputtering at the time when the atoms reach the substrate.

During the experiments, ideal vacuum conditions are maintained. We consider a graphene sheet lying in the xy plane (Fig. 4). Images *a* and *b* in Fig. 4 were extracted using Visual Molecular Dynamics [39].

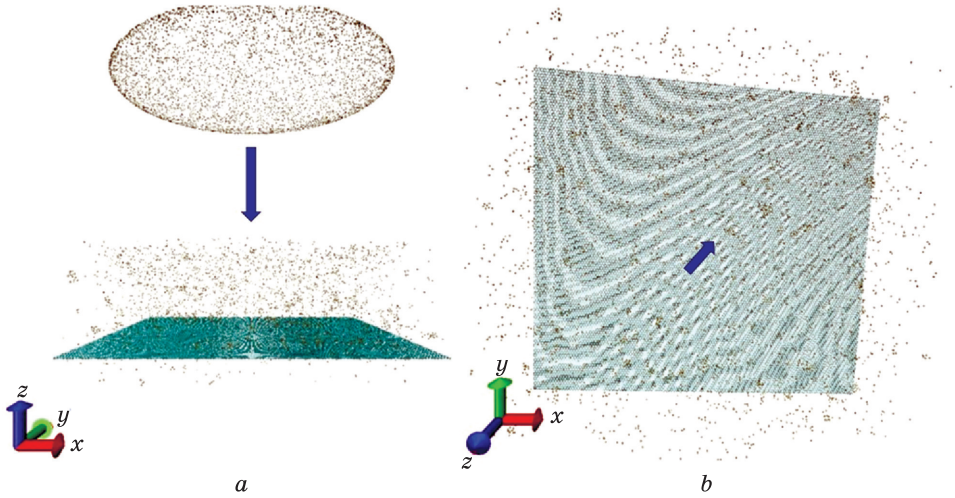

Fig. 4. Sputtering in the 'Surface Growth' mode, containing 10 000 palladium atoms at a temperature of 100 K: side (*a*) and top (*b*) views

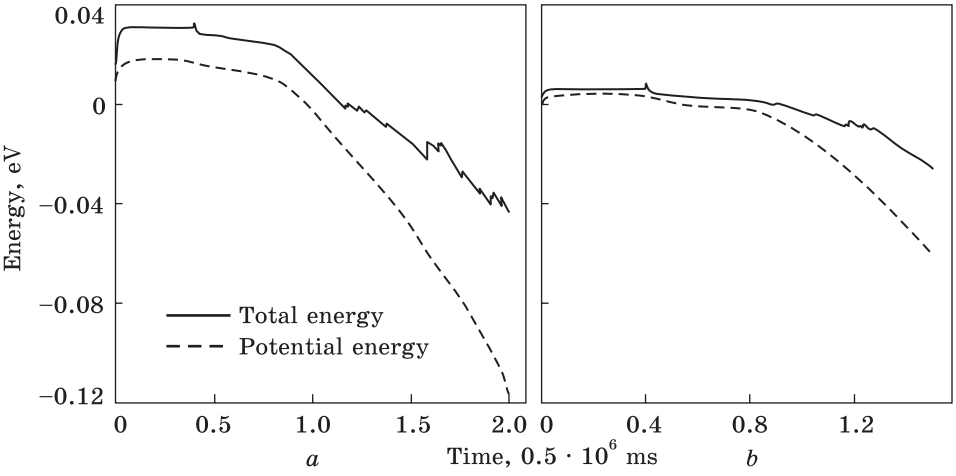

Fig. 5. Behaviour of total (solid line) and potential (dash line) energies over time for Pd, when sputtered with 10 000 atoms at a temperature of 100 K (*a*) and 20 K (*b*)

Strict conditions are established for boundary carbon atoms, it means they remain stationary throughout the simulation process. The total number of atoms participating in the study is 75 536. Of which 10 000 are the number of sputtered atoms, and the rest are part of a graphene sheet (64×64 cells).

In the simulation process, values such as the temperature T of the system, the lateral position X_{CM}, and the substrate force F_s, which is defined as the sum of the component forces acting on the metal atoms

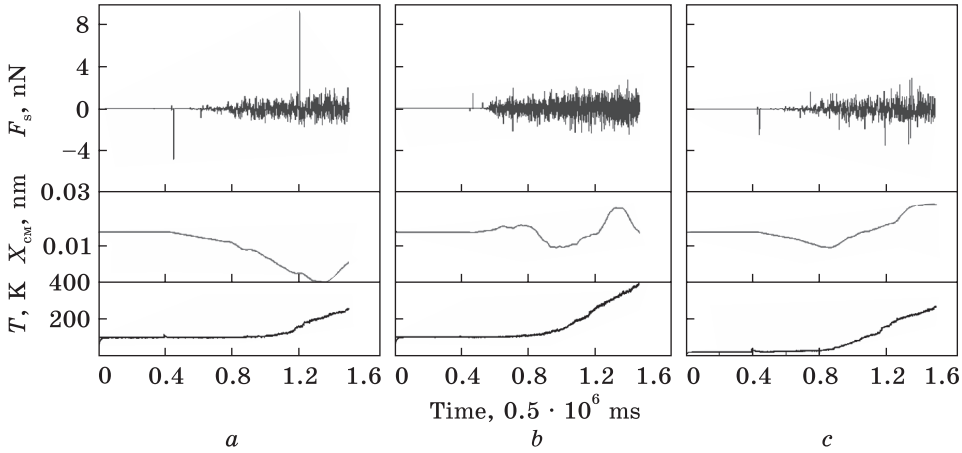

Fig. 6. Time-dependent temperature T, lateral position of X_{CM}, and force of substrate: (*a*) Al, at a sputtering of 10000 atoms; (*b*) Pd, when sputtered with 10000 atoms at a temperature of 100 K; (*c*) Pd, when sputtered with 10000 atoms at a temperature of 20 K

Table. **Comparison of temperature rise for experiments. Here, Pd1 is experiment with standard palladium sputtering settings; Pd2 — with adjusting the size of the substrate 32 × 32; Pd3 — with temperature setting 20 K; Pd4 — with the setting of the number of sputtered atoms 25000; Pd5 — with the adjustment of the energy of atoms of 0.6 eV**

Experiment	Initial temperature, K	Increase of temperature, K
Al	100	10
Au	100	20
Co	100	35
Ni	100	20
Pd1	100	40
Pd2	100	50
Pd3	20	15
Pd4	100	15
Pd5	100	15

from the carbon side, were calculated. Our code allowed us to sputter metal atoms on a graphene sheet, which facilitated a time-consuming approach to conducting experiments.

After 400000 steps, a ‘jump’ of total energy is observed in all sputterings, after which both potential and total energy begin to gradually decrease (Fig. 5). At this point, all variables begin to deviate from relatively stable previous values. The temperature rises sharply by 10 K to 50 K (Fig. 6), which is from 10% to 75% of the set temperature of the

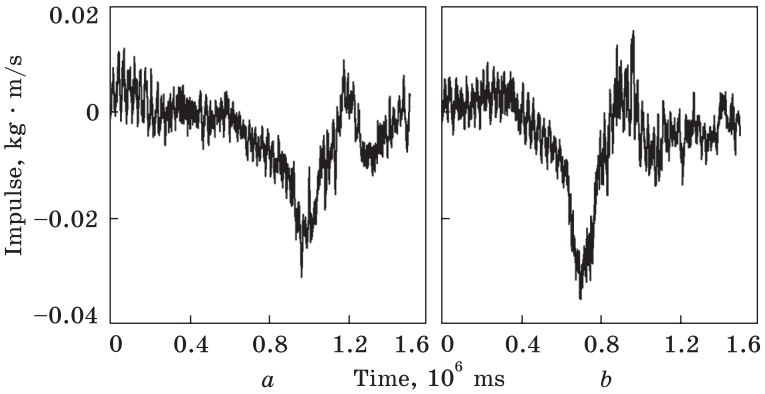

Fig. 7. Impulse behaviour depending on time: (*a*) Pd with the number of sputtered atoms 25000; (*b*) Pd with the atomic energy of 0.06 eV

experiment. The temperature rising for each of the experiments is described in Table. However, after a sharp increase, the temperature returns to the previous value and its further increase occurs over a long period of time at a slower rate (see Fig. 6).

The substrate force is heterogeneous. Up to a time interval of 400 000 steps, the value is zero. However, in the future, there is an alternation of zero values and deviations (see Fig. 6). The behaviour of the lateral position of the CM, after the moment of deviation from the initial value (in the most cases $1.48 \cdot 10^{-2}$ nm), for each experiment is unique (see Fig. 6).

A similar behaviour (as for X_{CM}) is also observed for the coordinate Y_{CM} of the centre of mass of the nanoparticle along the y-axis, the velocity of the centre of mass of the nanoparticle along the x-axis — Vel_X_{CM}, and y-axis — Vel_Y_{CM}. The trajectory of the saw tooth impulse graph begins to fluctuate with a decrease in average value (Fig. 7). The described changes in the system are observed approximately in the period when the atoms reach the graphene sheet. In addition, for each material and when correcting the settings of the experiments, similar behaviour is observed.

3.3. Behaviour of Al and Pd Nanoparticles

In this work, computer simulations were performed in the 'Surface Growth' mode to study the force of atomic friction of Pd and Al nanoparticles, with a number of 10 000 atoms, on a graphene sheet. We compare the obtained data for palladium sputtered at different temperatures. These experiments are conducted to study the substrate force and to understand the behaviour of atoms, which can provide useful information about tribological processes.

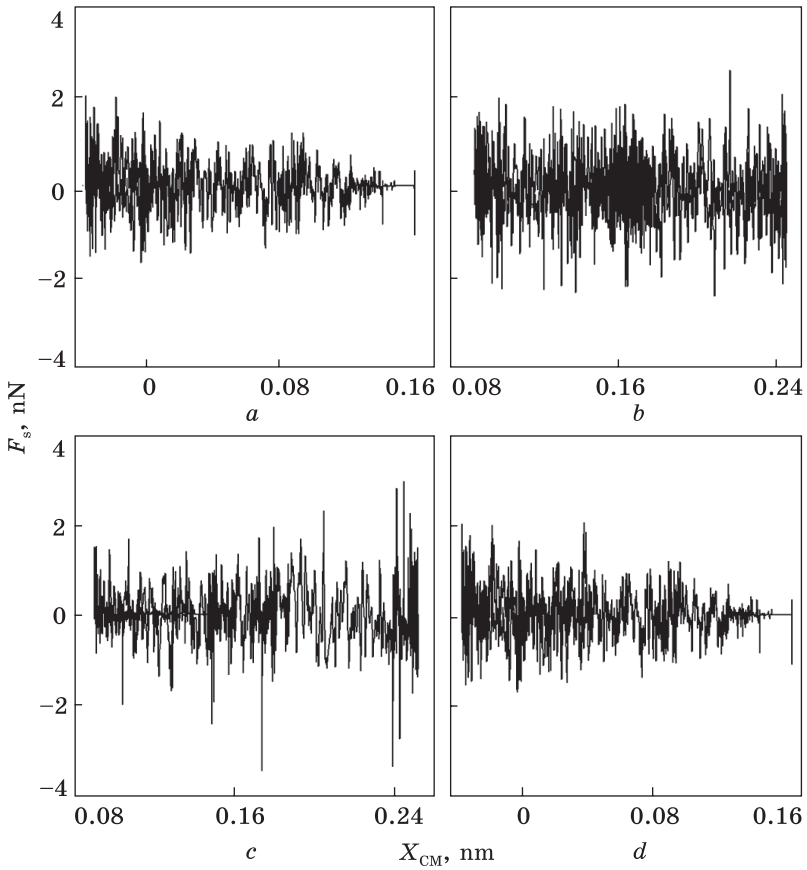

Fig. 8. Dependence of the substrate force on the lateral position of the centre of mass of nanoparticles: (*a*) Pd with a sputtering of 10000 atoms; (*b*) Al with a sputtering of 10000 atoms; (*c*) Pd at a temperature of 20 K; (*d*) Pd at a temperature of 100 K

Figure 6 shows a typical time dependence of the total values for the sputtering of Al and Pd from 10000 atoms. As mentioned in the previous section, after the start of sputtering X_{CM} is temporarily stable, but then we observe asymmetric deviations from the value of $1.5 \cdot 10^{-2}$ nm. These deviations change the sign like a sinusoid with increasing amplitude. Moreover, X_{CM} does not go beyond the range of values from $9 \cdot 10^{-3}$ nm to $2.5 \cdot 10^{-2}$ nm before increasing temperature. The substrate force F_s acting on the nanoparticle is not homogeneous. The time frequency of jumps may indicate intermittent slippage of the contact [40–44].

To find out the behaviour of the substrate force, consider Figs. 8 and 9, which show the dependences of F_s on X_{CM} for several Al and Pd sputtering. Figure 8 shows the dependence of the substrate force on the lateral position of the centre of mass of the nanoparticles. Figure 9 com-

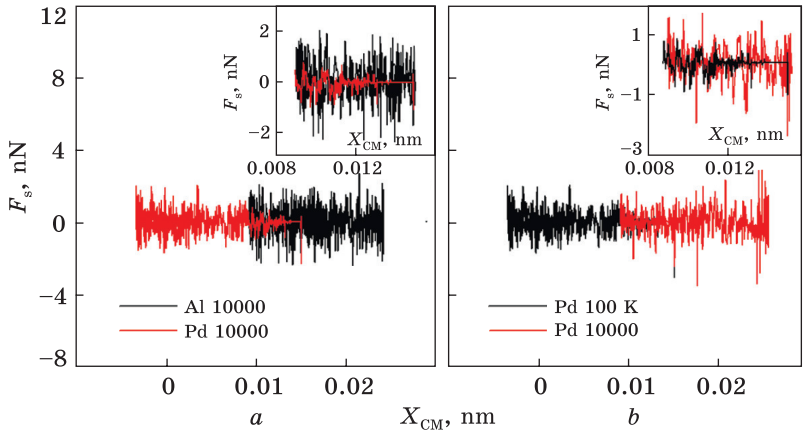

Fig. 9. Dependence of the substrate force on the lateral position of the centre of mass of nanoparticles: (*a*) Pd and Al with 10 000 atoms; (*b*) Pd at a temperature of 100 K and 20 K

pares these dependences, superimposing them as follows: (*a*) Pd with 10 000 and Al with 10 000 atoms; (*b*) Pd at a temperature of 100 K and 20 K. Also, the insets show enlarged areas with the interval of overlapping graphs. It can be seen that for Pd at 100 K, the difference between the mean amplitude and the global maximum is much larger than for other studies. The same situation is observed with the difference between the values of the average amplitude and the global minimum.

For the dependence of F_s on X_{CM} for Pd at a temperature of 20 K, the force of the substrate has an irregular shape and the spikes F_s are unevenly distributed, and for 100 K, the force of the substrate has a saw tooth shape and a more uniform distribution of spikes. For Pd, there is an irregular shape with uneven spikes, as well as decaying amplitude with a smaller range of values. The modulus of the lattice vector in graphene is equal to 0.246 nm and is compared with distance between maximal spikes, which may indicate the influence of the graphene lattice on the experimental behaviour. Note that positive values of F_s are observed, *i.e.*, the substrate force changes direction during sputtering. This indicates that the interaction of individual atoms with the graphene layer occurs in different directions [31, 45]. On average, at a temperature of 100 K, the amplitude of the peaks for Al is greater than for Pd. In addition, when comparing Pd at different temperatures, it can be noted that the frequency of spikes is irregular. At 100 K, it is slightly larger, and there is decaying amplitude. For 20 K, the modulus of the peak values is in a larger range. The symmetry of F_s values with respect to the abscissa axis is observed, which indicates the uniformity of the interaction of atoms with graphene in both directions. Returning to the

frequency of oscillations of the substrate force F_s, we can say that it is affected by the deformation of the substrate. That is, when sputtering of Pd at 100 K graphene sheet will undergo more deformation than in other described experiments.

3.4. Effect of Temperature, Energy, and Amount of Sputtering Atoms

This section compares the behaviour of a computer model in Surface Growth mode for several experiments to study the effect of initial system parameters such as the energy of the sputtered nanoparticles, their temperature, and the number of sputtered atoms. In order to find out how the energy of atoms affects the process of the computer modelling, experiments were compared in pairs, which examined the sputtering of aluminium and palladium with energy values of 0.03 eV and 0.06 eV.

In the course of work, comparing such parameters as impulse, temperature, lateral position of the centre of mass, total and potential en-

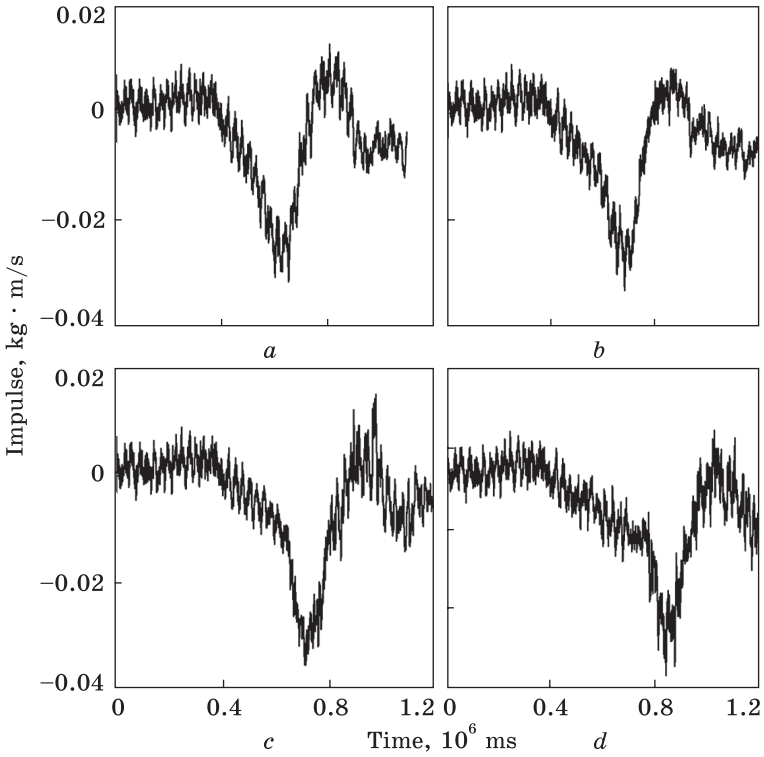

Fig. 10. Comparison of the behaviour of the impulse over time: (*a*) Al, at an energy of atoms of 0.06 eV; (*b*) Al, at an energy of atoms of 0.03 eV; (*c*) Pd, at an energy of atoms of 0.06 eV; (*d*) Pd, at an energy of atoms of 0.03 eV

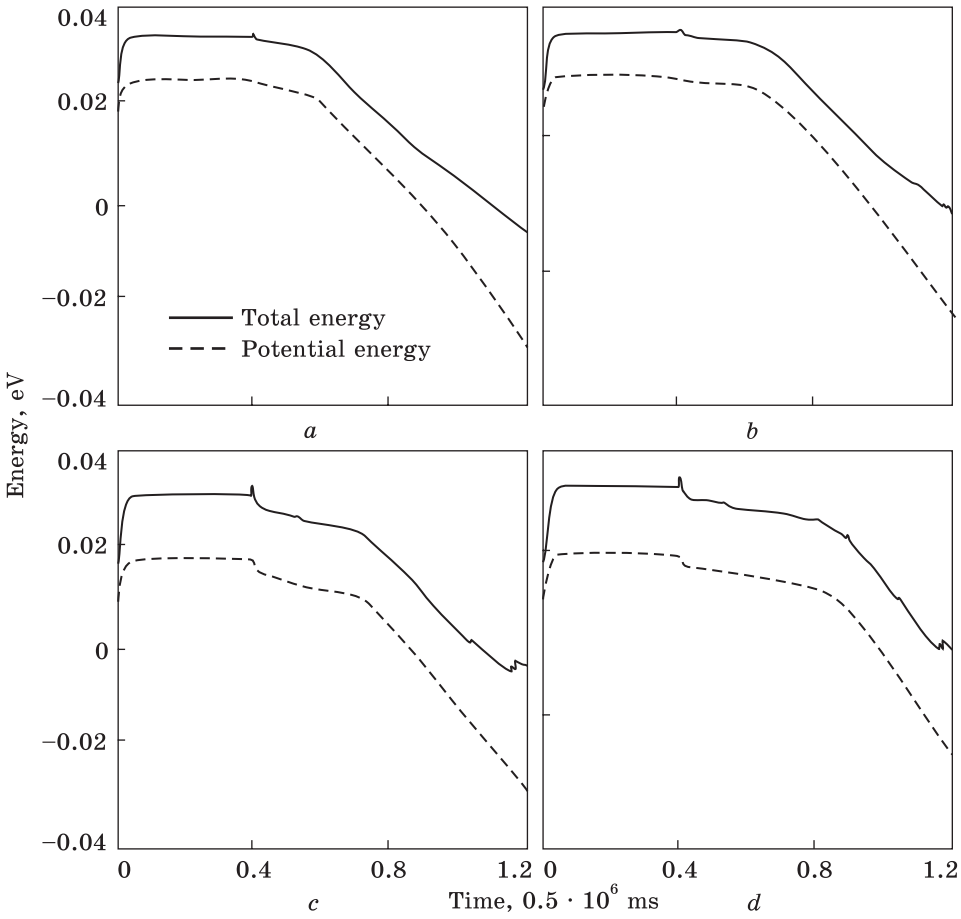

Fig. 11. Comparison of the time-dependent total (solid line) and potential (dash line) energies: (*a*) Al, at the energy of atoms of 0.06 eV; (*b*) Al, at an energy of atoms of 0.03 eV; (*c*) Pd, at an energy of atoms of 0.06 eV; (*d*) Pd, at an energy of atoms of 0.03 eV

ergy and substrate force, it was possible to observe that when the energy of atoms increases by 0.03 eV, the following changes are observed:

• the extremes of the saw tooth function of the impulse have shifted so that the trajectory has become more inclined; we can observe that the minimum and maximum were set approximately 500 time steps earlier for Al and 1000 time steps for Pd (Fig. 10);

• total and potential energies, during the interaction of atoms with the substrate, decreased by an average of approximately 0.005 eV (Fig. 11);

• the maximum temperature increased by 13 K for Al sputtering and by 17 K for Pd (Fig. 12);

• the lateral position of the centre of mass has a larger range of values; moreover, with increasing energy of atoms, we can observe a

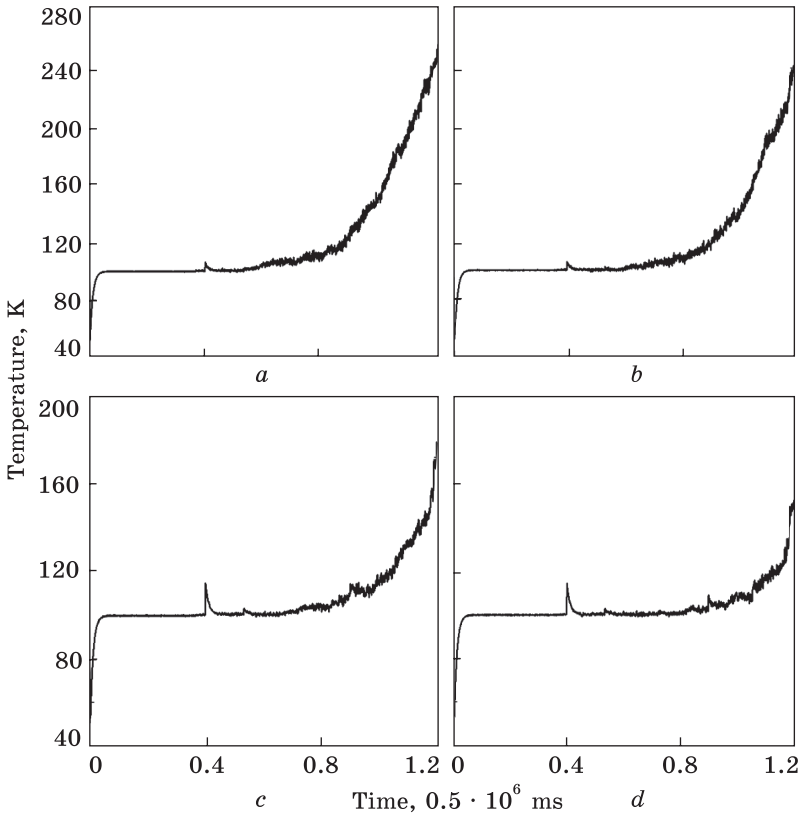

Fig. 12. Comparison of the temperature behaviour over time: (*a*) Al, at the energy of atoms of 0.06 eV; (*b*) Al, at the energy of atoms of 0.03 eV; (*c*) Pd, at the energy of atoms of 0.06 eV; (*d*) Pd, at the energy of atoms of 0.03 eV

general rapid increase in the lateral position of the CM relatively to time (Fig. 13);

• the behaviour of the substrate force changes with time; *viz.*, at the moment of reaching the substrate, the first atoms significantly reduce the spikes in the Pd sputter or disappear completely for Al (Fig. 14);

• the substrate force relative to the lateral position of the CM has a greater number of spikes (Fig. 15).

To find out how the initial temperature affects the sputtering process of the computer modelling, experiments were examined in pairs that examined the bombardment of graphene with aluminium particles at 100 K and 250 K and palladium at 20 K and 100 K. In the course of work, comparing such parameters as impulse, temperature, lateral position of the centre of mass and total and potential energy, it was possible to observe that when the initial temperature of the experiment increases by 150 K for Al and 80 K for Pd, the following changes are observed:

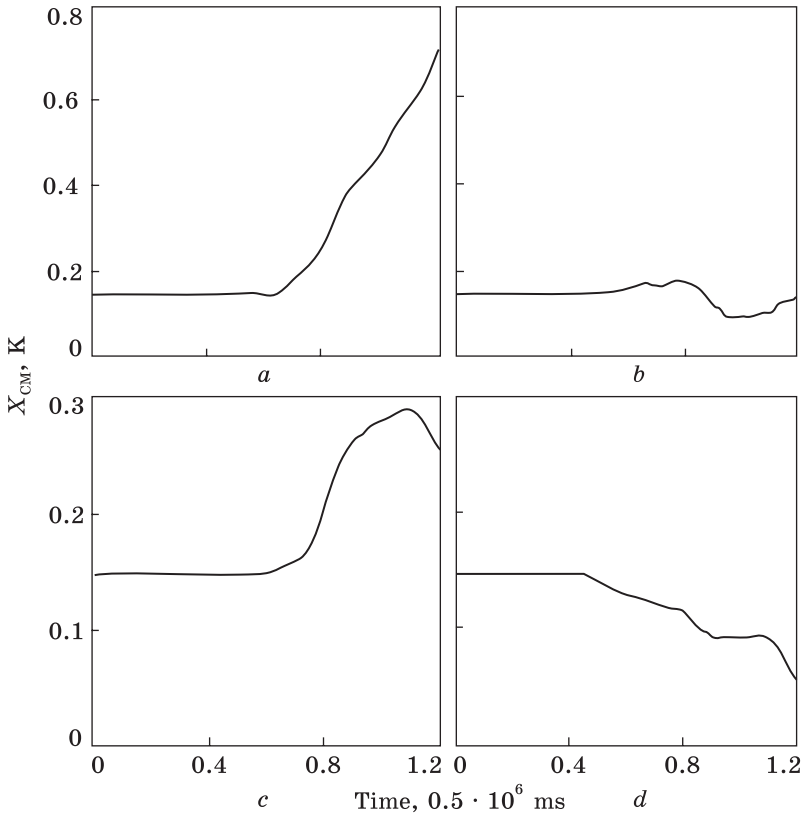

Fig. 13. Comparison of the behaviour of the lateral position of the CM over time: (*a*) Al, at the energy of atoms of 0.06 eV; (*b*) Al, at the energy of atoms of 0.03 eV; (*c*) Pd, at the energy of atoms of 0.06 eV; (*d*) Pd, at the energy of atoms of 0.03 eV

• uneven increase in the amplitude of the spikes of the saw tooth impulse graph (qualitatively compared with Fig. 10);

• the values of the extremums of the impulse graph increase, and the trajectory has a more inclined shape, see Fig. 10;

• the values of total and potential energies increase; for Al, the maximum total energy increased by 0.047 eV, and the potential energy increased by 0.027 eV; the minimum increased by 0.022 eV and 0.016 eV, respectively; for Pd, the maximum of total energy increased by 0.025 eV, and the potential by 0.0023 eV, the minimum increased by 0.014 eV and 0.007 eV, respectively (qualitatively compared with Fig. 11);

• energy graphs have a smoother trajectory, see Fig. 11;

• the rate increase in temperature during the experiment is inversely proportional to the initial temperature (qualitatively compared with Fig. 12); *i.e.*, if you reduce T_0 by half, the rate of temperature rise at the end of the experiment will increase by about 2 times; but this

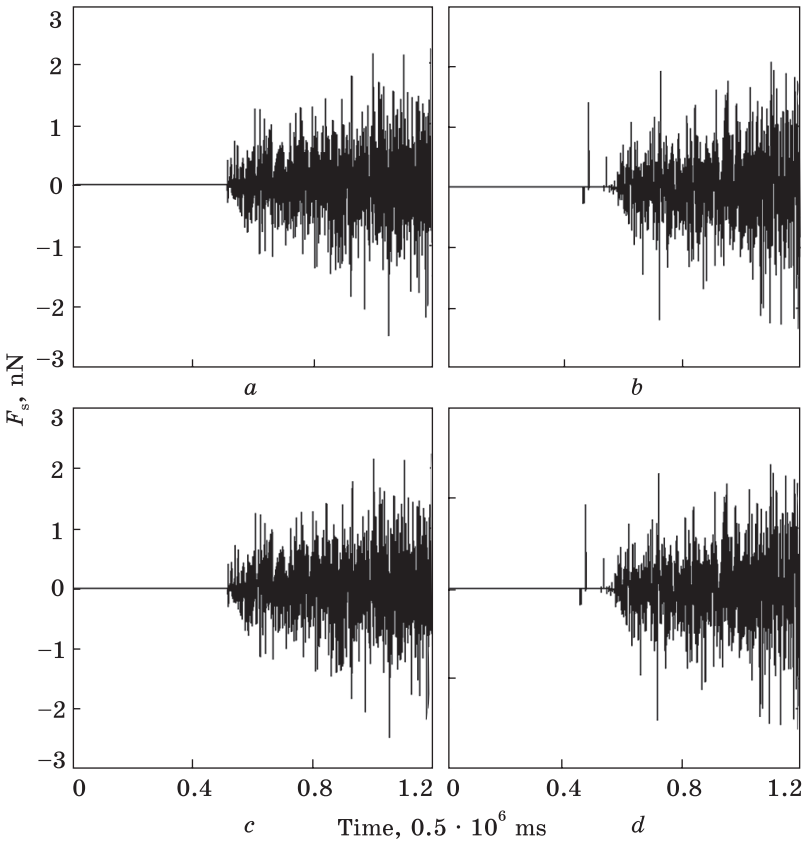

Fig. 14. Time dependence of the substrate force: (*a*) Al, at the energy of atoms of 0.06 eV; (*b*) Al, at the energy of atoms of 0.03 eV; (*c*) Pd, at the energy of atoms of 0.06 eV; (*d*) Pd, at the energy of atoms of 0.03 eV

does not mean that at any initial value of T_0 the final temperature will be the same for all experiments; in our case, the final value for Al increased by 6 K, and for Pd decreased by 3 K;

• slight increase in the range of values for the lateral position of the CM for Pd (0.0085 nm) and significant for Al (1.081 nm) (qualitatively compared with Fig. 13).

To study the effect of the number of sputtered nanoparticles, the sprays of Al with 10 and 20 thousands atoms and Pd with 10 and 25 thousands were compared. Thus, it was possible to observe that with an increase in the number of sputtered atoms (for Al by 10000, for Pd by 15000) changes are observed:

• the extremes of the impulse graph have become less pronounced, and the trajectory has a flatter shape (qualitatively compared with Fig. 10);

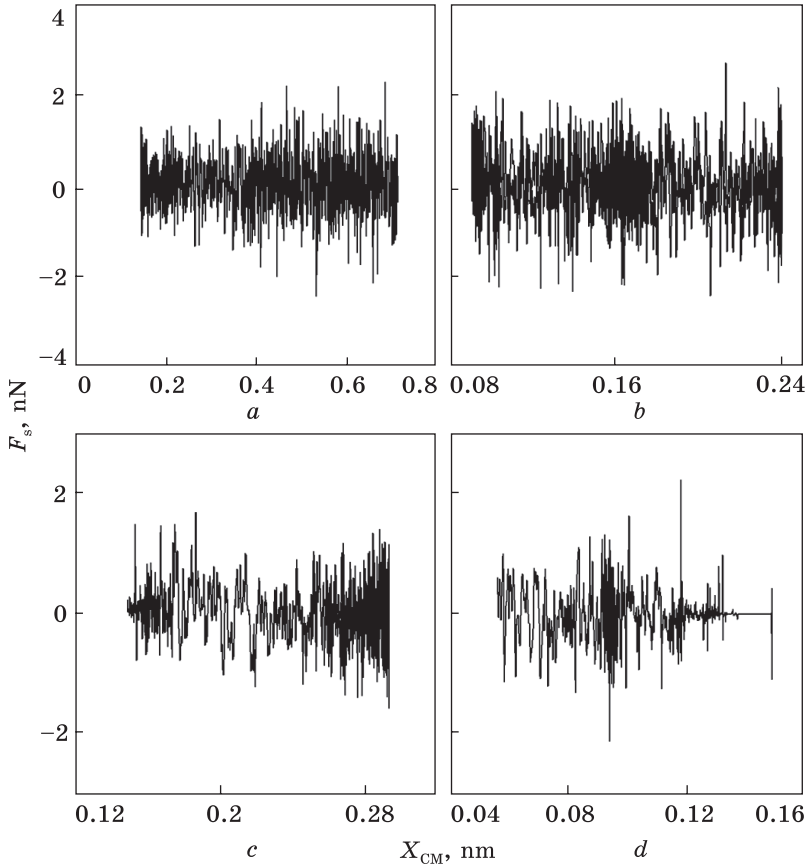

Fig. 15. Comparison of the behaviour of the substrate force on the lateral position of the CM: (*a*) Al, at the energy of atoms of 0.06 eV; (*b*) Al, at the energy of atoms of 0.03 eV; (*c*) Pd, at the energy of atoms of 0.06 eV; (*d*) Pd, at the energy of atoms of 0.03 eV

• energy has a smaller range of values, namely for Al the maximum remains unchanged, and the minimum of total energy increased by 0.0125 eV, potential one by 0.02 eV; for Pd, the increase in the minimum total energy is 0.01 eV, the potential one 0.03 eV (qualitatively compared with Fig. 11);

• temperature also has a decreasing range of values; thus, for Al the maximum decreased by 70 K, and for Pd by 36 K (qualitatively compared with Fig. 12);

• the behaviour of the substrate force with respect to time changes, namely, the spikes increase significantly at the time of arrival of the first atoms to the substrate (qualitatively compared with Fig. 14);

• there was also a more uniform distribution of the substrate force relative to the lateral position of the CM.

4. Conclusions

• The experimental methods of study of nanodimensional surfaces have been reviewed and compared. The practical applications of graphene have been described.

• Numerical calculations of sputtering of metal atoms on a graphene substrate by means of computer modelling by the method of molecular dynamics are made.

• The behaviour of nanoparticles was studied in order to analyse the interaction between graphene and sputters atoms. It is shown that there is a jump in total energy and temperature, as well as a change in the behaviour of the impulse and the substrate force when all sputters reach graphene atoms.

• The behaviour of time dependences of energy, temperature, impulse and substrate force, which is general to all experiments, is described.

• It is shown how the initial parameters (temperature, energy of nanoparticles, number of sputtered atoms) affect the behaviour of a computer-simulated system.

Acknowledgments. The Ministry of Education and Science of Ukraine support this study within the framework of the project 'Forming mechanisms and modelling of the structural steel of refractory slabs with predictive mechanical characteristics' (State Reg. No. 0122U000776) as well as visitor grant of Forschungszentrum-Jülich, Germany. The first author thanks Dr. Bo N.J. Persson for hospitality during his stay in Forschungszentrum-Jülich.

REFERENCES

1. *Fundamentals of Friction and Wear on the Nanoscale* (Eds. E. Gnecco and E. Meyer) (Cham: Springer: 2015); https://doi.org/10.1007/978-3-319-10560-4
2. A.V. Khomenko, N.V. Prodanov, K.P. Khomenko, and D.S. Troshchenko, Tribological properties of nanodimensional systems containing carbon surfaces, *J. Nano- Electron. Phys.*, **6**, No. 1: 01012 (2014).
3. A. Khomenko, M. Zakharov, and B.N.J. Persson, Frictional anisotropy of Al, Pt, and Pd Nanoparticles on a graphene substrate, *Tribol. Lett.*, **67**, No. 4: 113 (2019); https://doi.org/10.1007/s11249-019-1226-z
4. O. Mazur and L. Stefanovich, Pressure effect on the formation kinetics of ferroelectric domain structure under first order phase transitions, *Physica D*, **424**: 132942 (2021); https://doi.org/10.1016/j.physd.2021.132942
5. O.V. Fedchenko, A.I. Saltykova, and S.I. Protsenko, Influence of substrate on magnetoresistive and magneto-optical properties of Co/Fe film system, *J. Nano-Electron. Phys.*, **4**, No. 3: 03016 (2012).
6. A.D. Pogrebnjak, A.G. Ponomarev, A.P. Shpak, and Yu.A. Kunitskii, Application of micro- and nanoprobes to the analysis of small-sized 3D materials, nanosys-

tems, and nanoobjects, *Phys.-Usp.*, **55**, No. 3: 270 (2012); https://doi.org/10.3367/UFNE.0182.201203D.0287
7. G. Binnig and H. Rohrer, Scanning tunnelling microscopy, *Helvetica Phys. Acta*, **55**: 726 (1982); https://doi.org/10.5169/seals-115309
8. J.P. Spatz, S. Sheiko, M. Moller, R.G. Winkler, P. Reineker, and O. Marti, *Nanotechnology*, **6**: 40 (1995); https://doi.org/10.1088/0957-4484/6/2/002
9. R. Lüthi, E. Meyer, L. Howald, H. Haefke, D. Anselmetti, M. Dreier, M. Ruetschi, T. Bonner, R.M. Overney, J. Frommer, and H.-J. Güntherodt, Progress in nanocontact dynamic force microscopy, *J. Vac. Sci. Technol.*, **12**, No. 3: 1673 (1994); https://doi.org/10. 1116/1.587260
10. *Springer Handbook of Nanotechnology* (Ed. B. Bhushan) (Berlin–Heidelberg: Springer-Verlag: 2010); https://doi.org/10.1007/978-3-642-02525-9
11. I. Simon, A. Savitsky, R. Mülhaupt, V. Pankov, and C. Janiak, Nickel nanoparticle-decorated reduced graphene oxideWO_3 nanocomposite — a promising candidate for gas sensing, *Beilstein J. Nanotechnol*, **12**, No. 28: 343 (2021); https://doi.org/10.3762/bjnano.12.28
12. T.M. Radchenko, I.Yu. Sahalianov, V.A. Tatarenko, Yu.I. Prylutskyy, P. Szroeder, M. Kempiński, and W. Kempiński, The impact of uniaxial strain and defect pattern on magnetoelectronic and transport properties of graphene, *Handbook of Graphene: Growth, Synthesis, and Functionalization* (Eds. E. Celasco and A. Chaika) (Beverly, MA: Scrivener Publishing LLC: 2019), Vol. **1**, Ch. 14, p. 451; https://doi.org/10.1002/9781119468455.ch14
13. T.M. Radchenko, V.A. Tatarenko, and G. Cuniberti, Effects of external mechanical or magnetic fields and defects on electronic and transport properties of graphene, *Mater. Today: Proc.*, **35**, Pt. 4: 523 (2021); https://doi.org/10.1016/j.matpr.2019.10.014
14. T.M. Radchenko, I.Yu. Sahalianov, V.A. Tatarenko, Yu.I. Prylutskyy, P. Szroeder, M. Kempiński, and W. Kempiński, Strain- and adsorption-dependent electronic states and transport or localization in graphene, *Springer Proceedings in Physics: Nanooptics, Nanophotonics, Nanostructures, and Their Applications* (Eds. O. Fesenko and L. Yatsenko) (Cham, Switzerland: Springer: 2018), Vol. **210**, Ch. 3, p. 25; https://doi.org/10.1007/978-3-319-91083-3_3
15. P. Szroeder, I.Yu. Sagalianov, T.M. Radchenko, V.A. Tatarenko, Yu.I. Prylutskyy, and W. Strupiński, Effect of uniaxial stress on the electrochemical properties of graphene with point defects, *Appl. Surf. Sci.*, **442**: 185 (2018); https://doi.org/10.1016/j.apsusc.2018.02.150
16. P. Szroeder, I. Sahalianov, T. Radchenko, V. Tatarenko, and Yu. Prylutskyy, The strain- and impurity-dependent electron states and catalytic activity of graphene in a static magnetic field, *Optical Mater.*, **96**: 109284 (2019); https://doi.org/10.1016/j.optmat.2019.109284
17. X. Li, L. Tao, Z. Chen, H. Fang, X. Li, X. Wang, J.-B. Xu, and H. Zhu, Graphene and related two-dimensional materials: structure-property relationships for electronics and optoelectronics, *Appl. Phys. Lett.*, **4**: 021306 (2017); https://doi.org/10.1063/1.4983646
18. K.S. Novoselov and A.H. Castro Neto, Two-dimensional crystals-based heterostructures: materials with tailored properties, *Phys. Scr.*, **146**: 014006 (2012); https://doi.org/10.1088/0031-8949/2012/T146/014006
19. G.R. Bhimanapati, Z. Lin, V. Meunier, Y. Jung, J. Cha, S. Das, D. Xiao, Y. Son, M.S. Strano, V.R. Cooper, L. Liang, S.G. Louie, E. Ringe, W. Zhou, S.S. Kim,

R.R. Naik, B.G. Sumpter, H. Terrones, F. Xia, Y. Wang, J. Zhu, D. Akinwande, N. Alem, J.A. Schuller, R.E. Schaak, M. Terrones, and J.A. Robinson, Recent advances in two-dimensional materials beyond graphene, *ACS Nano*, **9**, No. 12: 11509 (2015); https://doi.org10.1021/acsnano.5b05556

20. V.B. Mohan, K.-T. Lau, D. Hui, and D. Bhattacharyya, Graphene-based materials and their composites: a review on production, applications and product limitations, *Composites Part B*, **142**: 200 (2018); https://doi.org/10.1016/j.compositesb.2018.01.013
21. T.M. Radchenko, V.A. Tatarenko, I.Yu. Sagalianov, and Yu.I. Prylutskyy, Configurations of structural defects in graphene and their effects on its transport properties, *Graphene: Mechanical Properties, Potential Applications and Electrochemical Performance* (Ed. Bruce T. Edwards) (New York: Nova Science Publishers, Inc.: 2014), Ch. 7, p. 219; https://novapublishers.com/shop/graphene-mechanical-properties-potential-applications-and-electrochemical-performance
22. A.G. Solomenko, R.M. Balabai, T.M. Radchenko, and V.A. Tatarenko, Functionalization of quasi-two-dimensional materials: chemical and strain-induced modifications, *Prog. Phys. Met.*, **23**, No. 2: 147 (2022); https://doi.org/10.15407/ufm.23.02.147
23. M. Neek-Amal, R. Asgari, and M. Tabar, The formation of atomic nanoclusters on graphene sheets, *Nanotechnology*, **20**, No. 13: 135602 (2009); https://doi.org/10.1088/0957-4484/20/13/135602
24. V.H. Crespi, Soggy origami, *Nature*, **462**: 858 (2009); https://doi.org/10.1038/462858a
25. N. Prodanov, *SurfaceGrowth: User Guide*; https://github.com/prodk/SurfaceGrowthConsole/blob/master/SurfaceGrowthConsole/SurfaceGrowthProto.h
26. M. Griebel, S. Knapek, and G. Zumbusch, *Numerical Simulation in Molecular Dynamics* (Berlin–Heidelberg: Springer-Verlag: 2007); https://doi.org/10.1007/978-3-540-68095-6
27. X.W. Zhou, H.N.G. Wadley, R.A. Johnson, D.J. Larson, N. Tabat, A. Cerezo, A.K. Petford-Long, G.D.W. Smith, P.H. Clifton, R.L. Martens, and T.F. Kelly, Atomistic scale structure of sputtered metal multilayers, *Acta Mater.*, **49**, No. 19: 4005 (2001); https://doi.org/10.1016/S1359-6454(01)00287-7
28. *ASM Handbook, Properties and Selection: Nonferrous Alloys and Special-Purpose Materials* (Metals Park, Ohio: ASM International: 1992), Vol. **2**.
29. N. Sasaki, K. Kobayashi, and M. Tsukada, Atomic-scale friction image of graphite in atomic-force microscopy, *Phys. Rev. B*, **54**: 2138 (1996); https://doi.org/10.1103/PhysRevB.54.2138
30. H. Berendsen, J. Postma, W. van Gunsteren, A. DiNola, and J. Haak, Molecular dynamics with coupling to an external bath, *J. Chem. Phys.*, **81**, No. 8: 3684 (1984); https://doi.org/10.1063/1.448118
31. A.V. Khomenko, N.V. Prodanov, and B.N.J. Persson, Atomistic modelling of friction of Cu and Al nanoparticles adsorbed on graphene, *Condens. Matter Phys.*, **16**, No. 3: 33401 (2013); https://doi.org/10.5488/CMP.16.33401
32. A.V. Khomenko, I.A. Lyashenko, and V.N. Borisyuk, Self-similar phase dynamics of boundary friction, *Ukr. J. Phys.*, **5**, No. 11: 1139 (2009).
33. W. Tian, X. Liu, and W. Yu, Research progress of gas sensor based on graphene and its derivatives: a review, *Appl. Sci.*, **8**, No. 7: 1118 (2018); https://doi.org/10.3390/app8071118

34. M. Vasilopoulou, L.C. Palilis, D.G. Georgiadou, A.M. Douvas, P. Argitis, S. Kennou, L. Sygellou, G. Papadimitropoulos, I. Kostis, N.A. Stathopoulos, and D. Davazoglou, Reduction of tungsten oxide: a path towards dual functionality utilization for efficient anode and cathode interfacial layers in organic light-emitting diodes, *Adv. Funct. Mater.*, **21**: 1489 (2011);
https://doi.org/10.1002/adfm.201002171
35. Q. Li, W. Liu, G. Cao, X. Li, and X. Wang, A study of gas sensing behaviour of metal-graphene contact with transfer length method, *Appl. Phys. Lett.*, **108**, No. 22: 221604 (2016);
https://doi.org/10.1063/1.4952619
36. P.T. Yin, S. Shah, M. Chhowalla, and K. Lee, Design, synthesis, and characterization of graphene–nanoparticle hybrid materials for bioapplications, *Chem. Rev.*, **115**, No. 7: 2483 (2015);
https://doi.org/10.1021/cr500537t
37. A. Mirzaei, S.S. Kim, and H.W. Kim, Resistance-based He_2S gas sensors using metal oxide nanostructures: a review of recent advances, *J. Hazard. Mater.*, **357**: 314 (2018);
https://doi.org/10.1016/j.jhazmat.2018.06.015
38. S. Ghosal and P. Bhattacharyya, A review on the sensing performances for three different ternary hybrid (Pd/RGO/TiO_2-NFs, Pd/RGO/MnO_2-NFs and Pd/RGO/WO_3-NFs) gas sensor device structure, *CSI Trans*, **8**: 117 (2020);
https://doi.org/10.1007/s40012-020-00299-z
39. W. Humphrey, A. Dalke, and K. Schulten, VMD: visual molecular dynamics, *J. Mol. Graphics*, **14**, No. 1: 33 (1996);
https://doi.org/10.1016/0263-7855(96)00018-5
40. A.V. Khomenko and I.A. Lyashenko, A stochastic model of stick-slip boundary friction with account for the deformation effect of the shear modulus of the lubricant, *J. Frict. Wear*, **31**: 308 (2010);
https://doi.org/10.3103/S1068366610040100
41. O.V. Yushchenko and A.Yu. Badalyan, Magnetic first-order phase transition in nano-cluster systems with the framework of Landau approximation, *J. Nano-Electron. Phys.*, **9**, No. 4: 04022 (2017);
https://doi.org/10.21272/jnep.9(4).04022
42. A.A. Goncharov, A.N. Yunda, H. Komsta, and P. Rogalski, Effect of structure on physicmechanical properties of transition metal diboride films, *Acta Phys. Pol. A*, **132**, No. 2: 270 (2017);
https://doi.org/10.12693/APhysPolA.132.270
43. A.V. Khomenko and I.A. Lyashenko, Temperature dependence effect of viscosity on ultrathin lubricant film melting, *Condens. Matter Phys.*, **9**, No. 4: 695 (2006);
https://doi.org/10.5488/CMP.9.4.695
44. A.V. Khomenko and I.A. Lyashenko, Hysteresis phenomena at ultrathin lubricant film melting in the gas of first-order phase transition, *Phys. Lett. A*, **366**, Nos. 1–2: 165 (2007);
https://doi.org/10.1016/j.physleta.2007.02.010
45. A.V. Khomenko, D.S. Troshchenko, L.S. Metlov, and P.E. Trofimenko, Features of the phase-kinetics of metals' fragmentation at the severe plastic deformation, *Nanosistemi, Nanomateriali, Nanotehnologii*, **15**, No. 2: 203 (2017);
https://doi.org/10.15407/nnn.15.02.0203

Received 03.03.2022;
in final version, 11.04.2022

О.В. Хоменко, А.А. Бєсєдіна, К.П. Хоменко, Р.Р. Чернущенко
Сумський державний університет,
вул. Римського-Корсакова, 2, 40007 Суми, Україна

КОМП'ЮТЕРНЕ МОДЕЛЮВАННЯ МЕТАЛЕВИХ НАНОЧАСТИНОК, АДСОРБОВАНИХ НА ГРАФЕНІ

За допомогою комп'ютерного моделювання досліджується вплив нанесених атомів Al, Pd, Co, Au, Ni на одношарову графенову підкладинку. Комп'ютерне моделювання розпорошення наночастинок на основі методу молекулярної динаміки реалізовано за технологією NVIDIA®CUDA™. За результатами модельних розрахунків досліджено загальну поведінку системи. Проведено експерименти з вивчення розпорошення атомів різних металів за різних початкових умов системи. На основі цих напорошень аналізується поведінка на початку взаємодії нанесених атомів з підкладинкою. Порівняно часові залежності латерального положення центру мас наночастинок і сили підкладинки протягом експерименту для різних матеріалів, що напорошуються. Досліджено поведінку повної та потенціальної енергій, температури й імпульсу системи. Показано, що спостерігається стрибок сумарної енергії та температури, а також зміна поведінки імпульсу та сили підкладинки при досягненні атомами Карбону графену для всіх осаджень.

Ключові слова: комп'ютерна модель, молекулярна динаміка, напорошення, графен, наночастинка, атомно-силова мікроскопія.